Biochimica et Biophysica Acta 1857 (2016) 1694–1704

Contents lists available at ScienceDirect

Biochimica et Biophysica Acta

journal homepage: www.elsevier.com/locate/bbabio

Membrane-bound electron transport systems of an anammox bacterium: A complexome analysis

Naomi M. de Almeida [a,*], Hans J.C.T. Wessels [b], Rob M. de Graaf [a], Christina Ferousi [a], Mike S.M. Jetten [a,c], Jan T. Keltjens [a], Boran Kartal [a,*,1]

[a] Department of Microbiology, Institute of Water and Wetland Research, Radboud University Nijmegen, 6525 AJ Nijmegen, The Netherlands
[b] Nijmegen Center for Mitochondrial Disorders, Radboud Proteomics Center, Translational Metabolic Laboratory, Department of Laboratory Medicine, Radboudumc, Geert Grooteplein-Zuid 10, 6525 GA Nijmegen, The Netherlands
[c] Kluyver Laboratory for Biotechnology, Delft University of Technology, Julianalaan 67, 2628 BC, Delft, The Netherlands

ARTICLE INFO

Article history:
Received 29 April 2016
Received in revised form 14 July 2016
Accepted 19 July 2016
Available online 25 July 2016

Keywords:
Anaerobic ammonium oxidation (anammox)
Complexome profiling
Blue Native gel electrophoresis
Respiratory complexes

ABSTRACT

Electron transport, or oxidative phosphorylation, is one of the hallmarks of life. To this end, prokaryotes evolved a vast variety of protein complexes, only a small part of which have been discovered and studied. These protein complexes allow them to occupy virtually every ecological niche on Earth. Here, we applied the method of proteomics-based complexome profiling to get a better understanding of the electron transport systems of the anaerobic ammonium-oxidizing (anammox) bacteria, the N_2-producing key players of the global nitrogen cycle. By this method nearly all respiratory complexes that were previously predicted from genome analysis to be involved in energy and cell carbon fixation were validated. More importantly, new and unexpected ones were discovered. We believe that complexome profiling in concert with (meta)genomics offers great opportunities to expand our knowledge on bacterial respiratory processes at a rapid and massive pace, in particular in new and thus far poorly investigated non-model and environmentally-relevant species.

1. Introduction

Respiration is a quintessential property of most forms of life. This principle, also known as electron transport (ETP) or oxidative phosphorylation (OXPHOS), was comprehensively formulated in his seminal paper by Peter Mitchell just fifty years ago [1]. Herein, electrons derived from the oxidation of primary electron donors are transferred via one or more (membrane-bound) Respiratory Complexes (RCs) to a terminal electron acceptor [2]. Low-molecular weight mobile carriers dissolved in the cytoplasm (NADH, ferredoxins), in the membrane (quinones) or in the periplasmic solute (*c*-type cytochromes or blue copper proteins (BCPs)) act as electron shuttles in between the RCs. These systems are organized in such a way that the energy released in these redox processes is conserved as a proton- (or sodium-) motive force (*pmf* or *smf*) across a cell membrane. This force drives the synthesis of ATP by a H^+ (or Na^+)-dependent membrane-bound ATP synthase (ATPase, complex V).

The canonical example for an oxidative phosphorylation system is the mitochondrion of Eukaryotes. In mitochondria, electrons from NADH and succinate oxidation are transferred through NADH dehydrogenase (NDH-1, complex I) and succinate dehydrogenase (complex II), respectively, and via a Rieske/cytochrome *b*-type RC (quinol:cytochrome *c* oxidoreductase, R/*b*, Complex III) to the terminal oxidase (complex IV) that reduces O_2 to H_2O. Eukaryotes are generally limited to oxygen-dependent (aerobic) respiration. In contrast, Prokaryotic organisms can use, in species-dependent ways, a vast variety of inorganic or organic electron donors and acceptors in their aerobic or anaerobic energy metabolism, each type of redox substrate requiring its dedicated RCs. Part of these processes have been studied extensively over the years and are covered in textbooks. Still, we have a limited understanding of respiratory processes and their variations in Prokaryotes, especially due to the fact that only a small subset

Abbreviations: 2DE, two-dimensional gel electrophoresis; anammox, anaerobic ammonium oxidation; (F-, N-, V-)ATPase, proton-pumping F_1F_o-, (hypothetical) sodium-pumping, and vacuolar-ATPase, respectively; BCP, blue copper protein; OXPHOS, oxidative phosphorylation; BNE, Blue Native gel electrophoresis; ETM, electron transfer module; FDH, formate dehydrogenase; HAO, hydroxylamine oxidoreductase; HDH, hydrazine dehydrogenase; HZS, hydrazine synthase; LC-MS/MS, liquid chromatography coupled to on-line tandem mass spectrometry; MALDI-TOF, matrix assisted laser desorption ionization time-of-flight; MS, mass spectrometry; NDH (NUO), NADH dehydrogenase; NADH, quinone oxidoreductase (complex I); NQR, (sodium pumping) NADH:quinone oxidoreductase; NXR, nitrite:nitrate oxidoreductase; NXRmemb, membrane-bound protein complex associated with the NXR system; *pmf*, proton-motive force; Q-pool, quinone pool; R/b, Rieske:heme b respiratory complex (quinol:cytochrome *c* oxidoreductase Complex III); RC, respiratory complex; Rnf, Na^+ (or H^+)-translocating NAD^+:ferredoxin oxidoreductase; RPKM, reads per kilobase per million; *smf*, sodium-motive force; TMH, transmembrane-spanning helix.

* Corresponding authors.
E-mail addresses: almeida@science.ru.nl (N.M. de Almeida), bkartal@mpi-bremen.de (B. Kartal).
[1] Present address: Microbial Physiology Group, Max Planck Institute for Marine Microbiology, Celsiusstr. 1, D-28359 Bremen, Germany.

http://dx.doi.org/10.1016/j.bbabio.2016.07.006
0005-2728/

(<1%) of these organisms have been cultured [3]. Recent advances in nucleotide-sequencing technologies allowed for mass data collection on environmental samples. Such (meta)genomic studies show an overwhelming variety of RCs in unknown prokaryotes (for example, see [4–15]). Nevertheless, a genomic analysis only provides a blueprint of the physiological capabilities of an organism. Further, translated protein sequences from these (meta)genomes can identify proteins homologous to enzymes with already known functions. As such, these analyses aid in the formulation of new hypotheses, but they cannot directly lead to the discovery of new functions of enzymes or novel assemblies of different proteins into functional complexes, as it is typical for RCs.

One such group of microorganisms to which the above considerations apply is the anaerobic ammonium-oxidizing (anammox) bacteria. In fact, *Kuenenia stuttgartiensis*, the organism used in this study, was one of the first organisms whose genome was sequenced and assembled using a metagenomic approach [16]. The discovery of anammox bacteria caused a paradigm shift in our understanding of the biogeochemical nitrogen cycle [17]. These organisms derive their energy for autotrophic growth from the oxidation of ammonium with nitrite as terminal electron acceptor to produce N_2 as the end product [16,18]. Because of the presumed inert nature of ammonium under anoxic conditions, this process was deemed impossible for many years. Nevertheless, following their first detection in an anaerobic wastewater treatment plant [19], anammox bacteria have been detected in virtually every environment where fixed nitrogen compounds are degraded anoxically [20,21]. It has been estimated that 30–70% of all N_2 emitted into the atmosphere is the result of anammox activity [22,23]. Besides its ecological relevance, application of this process offers an environment-friendly and cost-effective alternative to conventional wastewater treatment for the removal of ammonium [24].

Insights from the metagenome of *K. stuttgartiensis*, supported by physiological and biochemical studies, enabled the proposal of how anammox bacteria make a living from anaerobic ammonium oxidation (Fig. 1) [16,25,26]. In essence, the anammox catabolism is comprised of three consecutive reactions catalysed by (1) a nitrite reductase producing nitric oxide (NO) known from many other bacteria, (2) hydrazine synthase (HZS), a biochemical novelty [25–27], that combines ammonium and NO together with the input of three electrons to form the unique intermediate hydrazine (N_2H_4), and (3) hydrazine dehydrogenase (HDH) [28], an octaheme protein related to hydroxylamine oxidoreductase (HAO) from aerobic ammonium-oxidizing bacteria [29,30]. These three are soluble, i.e. not membrane-bound, enzymes and are localized inside a special cell organelle, the anammoxosome, representing another unique feature of the anammox bacteria [31,32]. Regarding energy conservation, it is thought that the (four) electrons that originate from hydrazine oxidation feed the reduced quinone (quinol, Q-) pool by the action of an as yet-unknown oxidoreductase (Fig. 1). Consequently, quinol oxidation would provide the electrons for hydrazine synthesis and nitrite reduction. These two reactions would be mediated by an electron transfer module (ETM) encoded in the HZS gene cluster and by a Rieske/cyt *b*-type RC, respectively. The net result is a cyclic flow of electrons, establishing a *pmf* for ATP synthesis. The scheme shown in Fig. 1 can only be a simplified one: The genome of *K. stuttgartiensis* [16] and other anammox genomes that have been sequenced by now [33–38] suggested a most puzzling redundancy of RCs, including four different ATPases, three variants of complex III, several multiprotein complexes related to complex I and a wide range of *c*-type cytochromes. In addition, the scheme (Fig. 1) does not account for the way NADH and reduced ferredoxins needed for cell carbon synthesis are generated. In anammox bacteria, anabolism relies on CO_2 fixation by the Wood-Ljungdahl pathway [16,25,26]. Next to this, NAD^+ and ferredoxin reduction will have to tap from the cyclic electron flow and the electron pool has to be replenished. This replenishing is accomplished by nitrite oxidation to nitrate, which is catalyzed by an unusual nitrite:nitrate oxidoreductase (NXR) [39,40] and is associated with cell growth [41]. It is, however, unknown how the electrons from nitrite oxidation are shuttled into the anammox cycle.

To get an insight into the extent RCs predicted from genomic analysis of *K. stuttgartiensis* are expressed at the protein level, how different gene products form distinct complexes, to find further support for the hypothetical mechanism shown in Fig. 1, and to detect missing or unexpected links that challenge the current hypotheses, we now made a comprehensive analysis of the membrane proteome of this unique bacterium using the complexome profiling approach [42]. Thus far, this approach has been almost exclusively applied in mitochondrial research focusing on the elucidation of assembly factors in otherwise structurally well-studied OXPHOS complexes [43–46] and very recently also in the identification of some RCs of a sulfate-reducing bacterium [47]. In this method, protein complexes are carefully dissolved from the membranes and separated by Blue Native Gel Electrophoresis

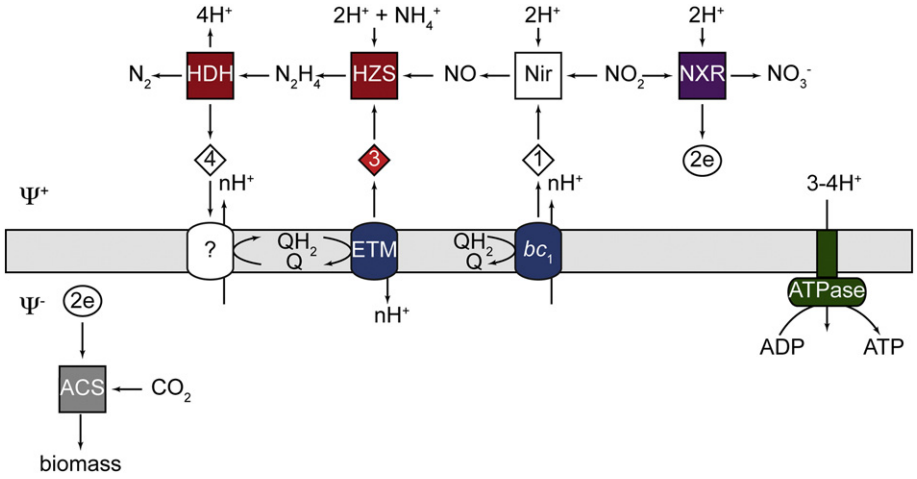

Fig. 1. Genome-based overview of processes involved in the anammox reactions, ATP synthesis and carbon fixation in *K. stuttgartiensis*. Electrons from hydrazine oxidation were proposed to reduce the quinone- (Q) pool *via* a hypothetical quinone reductase (indicated by a question mark). The Q-pool supplies electrons for the reductive steps of the anammox process. ACS, CO dehydrogenase/acetyl-CoA synthase, representing carbon fixation according to the reductive acetyl-CoA pathway; ATPase, ATP synthase; bc_1: quinol:cytochrome *c* oxidoreductase (bc_1 complex); ETM, putative electron transfer module from the Q-pool to HZS; HDH, hydrazine dehydrogenase; HZS, hydrazine synthase; Nir, nitrite reductase; NXR, nitrite:nitrate oxidoreductase. White shapes indicate proteins with no identified candidate; red diamond, putative cytochrome *c* protein. Numbers refer to the number of electrons that are transferred. Ψ^+ and Ψ^-: positive and negative sides of the electrochemical gradient (inside and outside of the anammoxosome, respectively).
Adapted from [26].

(BNE). After separation, gels are cut in multiple pieces that are subjected separately to shotgun proteomics. Hierarchical clustering of migration profiles then allows the identification of protein complexes composed of co-migrating subunits. As the result of this study, the presence of many predicted RCs was validated. Moreover, based on the detection of new and unexpected protein complexes, the results also provided new insights on the energy and carbon metabolism of anammox bacteria. Altogether, complexome profiling is fully complementary to (meta)genomics and transcriptomics, and offers a powerful tool to achieve comprehensive and fundamental understanding of microbial bioenergetics and the unexplored versatility that lies therein.

2. Materials and methods

2.1. Cell growth and sample preparation

Kuenenia stuttgartiensis was grown as planktonic cells in a 10-l membrane reactor [25]. The cell pellet of 1 l of cell culture (OD_{600} ~ 1.2) was resuspended in 7 ml of sample buffer containing 20 mM potassium phosphate buffer (pH 7.0), 0.75 M 6-aminocaproic acid, 10% (w/v) glycerol. This and all next steps were performed at 4 °C unless specified otherwise. Cells were disrupted by three passages through a French pressure cell operated at 138 MPa at room temperature. Cell debris was removed by centrifugation (4500 *g*, 15 min) and the supernatant was subjected to an ultracentrifugation step (184,000 *g*, 1 h). The clear red supernatant comprising the soluble proteins was discarded and the pellet containing the membrane fraction was washed three times by subsequent dilution in sample buffer and ultracentrifugation to yield a colorless supernatant. The pellet was resuspended in 7 ml sample buffer. To dissolve membranes, β-laurylmaltoside was added to the sample in a protein to detergent ratio of approximately 1:6 (w/w), and this mixture was incubated on a rotator for one hour. Protein quantification was performed using the 2-D Quant Kit according to the product manual (GE Healthcare, USA), with bovine serum albumin as standard.

The optimal and reproducible resolution of the protein complex migration patterns relies on the careful but efficient dissolving of the membranes without disintegrating native membrane-embedded protein complexes [48]. This resolution requires the presence of a suitable mild detergent in the optimal amounts under the optimal conditions. In preliminary setups, first dimension BNE gel lanes (Section 2.2.1.) were resolved in a second dimension by SDS-PAGE (2DE) (Section 2.2.2) and protein spots were identified by matrix assisted laser desorption ionization time-of-flight mass spectrometry (MALDI-TOF MS) (Section 2.3.2) to get a broad impression of the proteins present the first-dimension BNE gel bands. The protein migration pattern of the most abundant protein in the membrane preparations, a putative porin (kustd1878) [49] was used to ensure that a sufficient amount of detergent was added to dissolve the membranes completely while keeping membrane-bound protein complexes intact (Supporting information, Fig. S1). Insufficient dissolution treatment was judged by a smeary band of the porin subunit on a 2D-gel.

2.2. Gel electrophoretic methods

2.2.1. Blue Native polyacrylamide gel electrophoresis (BNE)

BNE of membrane protein complexes was performed as described by [48,50], using pre-casted 4–16% and 3–12% linear polyacrylamide gradient gels (Invitrogen, USA). Prior to loading, 1 μl of sample additive (0.75 M 6-aminocaproic acid, 5% Serva Blue G) was added to 40 μg membrane protein sample. Gels were run at room temperature at 100 V until the migration front reached the end of the gel. Cathode and anode buffers were prepared according to the supplier's protocol (Invitrogen, USA). All gels were routinely stained with a ready-to-use Colloidal Coomassie Blue Stain (Severn Biotech Ltd., USA) and destained with demineralized water. After electrophoresis, BNE gel lanes were analyzed in two ways. (1) Gel lanes were assembled onto an SDS-PAGE gel and separated by electrophoresis in the second dimension (2DE) (Section 2.2.2.) after which proteins of interest were identified by MALDI-TOF MS (Section 2.3.2.). (2) Gel lanes were cut into 65 or 66 equally sized slices. After in-gel tryptic digestion of the slices (Section 2.3.1), each of these was subjected to proteolytical analysis by liquid chromatography coupled to on-line tandem mass spectrometry (LC-MS/MS) (Section 2.3.3).

2.2.2. Second dimension SDS-PAGE

Duplicate BNE lanes were assembled onto second dimension 10% SDS-PAGE as published previously [51] with minor modifications: second dimension gels were 1 mm thick and the acrylamide in the stacking gel was replaced with 0.5% agarose. Protein spots were picked and plugs were, after in-gel tryptic digestion, analyzed by MALDI-TOF mass spectrometry.

2.2.3. Molecular mass estimation of protein complexes

For mass estimation of protein complexes in the BN gels, a high molecular weight marker (Invitrogen, USA) was used. The linear range for molecular weight estimations was 146–720 kDa (Supporting information, Fig. S2). It should be noted that BN protein complexes may migrate differently from native complexes and membrane proteins may be associated with substantial amounts of lipids and detergent, hampering a reliable estimation of molecular masses of the protein constituents in the BN complexes [48,50].

2.3. Mass spectrometric methods

2.3.1. Tryptic digestion

Gel slices and gel plugs from 2D BN PAGE gels were washed and dehydrated with 50% and 100% acetonitrile, respectively, and rehydrated in 50 mM ammonium bicarbonate until they became colorless. Protein reduction was performed by addition of 10 mM DTT at 56 °C for 30 min, followed by an alkylation incubation in 50 mM 2-chloroacetamide [53] for 30 min in the dark at room temperature. Proteins were digested as described elsewhere [51] and peptides were extracted in 10 μl 0.1% TFA by 20 s sonication followed by 20 min incubation at room temperature. Hereafter, the gel pieces were dehydrated in 10 μl 100% acetonitrile. Both aqueous and acetonitrile fractions were combined and desalted using *in-house* constructed STAGE tips. The elute was used for mass spectrometric analyses.

2.3.2. MALDI-TOF MS

MALDI-TOF MS analysis was performed as described in detail by [51]. In brief, 0.5 μl of a digested peptide solution was spotted onto a MALDI-TOF MS ground steel plate and covered with 0.5 μl of a 10 $mg \cdot ml^{-1}$ α-cyano-4-hydroxycinnamic acid in 50% acetonitrile and 0.05% TFA mixture. Measurements were performed on a Bruker Biflex III mass spectrometer (Bruker Daltonik, Germany), operating in the reflectron mode. Monoisotopic peaks in the range of m/z 600–3000 were manually selected, using the Biotools software, and exported to the Mascot Peptide Mass Fingerprint search tool (Matrix Science). An *in-house in silico* predicted proteome database of *K. stuttgartiensis* was used for protein identification, allowing carbamidomethylation as a fixed and methionine oxidation as a variable modification, and 0.2 Da peptide mass tolerance and a single missed cleavage by trypsin.

2.3.3. LC-MS/MS analysis

Proteomic analysis of the BNE fractions by LC-MS/MS was performed as detailed before [51] with some minor modifications. Measurements took place on a nanoflow liquid chromatography system (Easy nLC, Thermo scientific, Germany) coupled online *via* a nanoflow electrospray ionization source (Nanospray Flex Ion Source, Thermo scientific, Germany) to a linear ion trap Fourier transform ion-cyclotron-resonance

mass spectrometer (7Tesla LTQ FT Ultra, Thermo scientific, Germany). For chromatographic separations an Acclaim PepMap trap column (5 μm particle size 100 Å pore 0.3 × 5 mm, Thermo scientific, Germany) was used in combination with a 15 cm long 100 μm ID electrospray emitter (PicoTip emitter FS360-100-8-N-5-C15, New Objective) that was packed *in-house* with reversed phase material (3 μm particle size 120 Å pore C18-AQ ReproSil-Pur, Dr. Maisch GMBH, Germany) as analytical column; details regarding the performance of the system can be found in [52]. Samples were loaded onto the trap column at 250 bar using 0.1% formic acid. Peptides were eluted from the column in 60 min using a linear gradient of 7–35% acetonitrile in 0.1% formic acid at a flow rate of 300 nl min^{-1}. The mass spectrometer was operated in positive ion mode and was set to acquire a high resolution full MS scan by the ion-cyclotron-resonance cell (100.000 resolving power at 400 *m/z*, 1 microscan, 1E6 ions, 2500 ms maximum injection time) with up to 4 fragmentation experiments in parallel by the linear ion trap (normal resolution, 1 microscan, 3000 ions, 750 ms maximum injection time, 27% normalized collision energy, 30 ms activation time) for each duty cycle. Redundant analyses of eluting peptides in collision induced dissociation experiments were minimized using dynamic exclusion (500 list size, 5 min exclusion time) in combination with early expiration (2 S/N, 10 spectra). Further details on the MS analyses and statistics can be found in Supplemental information Table S1.

2.4. Data processing and complexome profiling

Acquired raw data files from LC-MS/MS runs were processed using the MaxQuant software with default settings for FTMS full MS scans and ion-trap MS/MS scans data processing [54]. Label-free quantitation (LFQ) was performed using 'match between runs' in a 0.5-min time window. Database searches of the MS/MS data against the RefSeq *K. stuttgartiensis* fasta protein sequence database allowed for a 6 ppm precursor mass error and 0.5 Da fragment ion mass error. For validation purposes, a maximum false discovery rate of 1% was allowed, both at the peptide and protein levels. Only razor and unique peptides were used for label-free protein quantitation. Protein abundance values were calculated as intensity-based absolute quantitation (iBAQ) values. Output from MaxQuant was further processed manually to obtain relative abundance profiles for identified proteins. For visualization (heat maps) and clustering purposes, profiles were normalized, i.e. scaled between 0 and 1. To identify proteins that co-migrated in the BNE gels, normalized protein abundance profiles were subjected to hierarchical clustering analysis based on Pearson's uncentered correlation as distance metric (complete linkage) with optimized tree leaf order as exemplified in Supporting information Fig. S3A, using the MeV software package [55]. No additional smoothing or filtering was applied to the obtained electrophoretic migration profiles. Only proteins with ≥2 razor and unique peptides were used to construct protein profiles. Hydrazine synthase (kuste2859–61) and ATPase-I (kuste3787–96) subunits were used to validate correct profiling (Supporting information, Fig. S3C). The mass spectrometry proteomics data have been deposited to the ProteomeXchange Consortium via the PRIDE partner repository with the dataset identifier PXD004566.

2.5. Quinone analysis

All solvents used were purchased from Merck, Germany and were of HPLC grade. For quinone identification, Ubiquinone 10 (UQ10) (Sigma-Aldrich, USA) and Menaquinone 4 (MK4) (Supelco, USA) served as references. All steps were performed at room temperature, unless mentioned otherwise. Four portions of 100 mg freeze-dried cells each kept in a 1.5-ml reaction tube containing a 5/32″ steel ball were grinded with a Retsch MM 300 mixer mill at 30 Hz for 2 min. To each of the grinded samples, 500 μl ultrapure water and 300 μl pentane were added, after which mixtures were vortexed for 2 min and centrifuged at maximum speed in a bench top centrifuge for 5 min. After collection of the upper pentane phase and the addition of 300 μl of pentane to the lower (aqueous) phase, the extraction procedure was repeated as described. Both pentane phases were combined and brought to dryness under a nitrogen flow. Dried extracts were dissolved in 200 μl methanol/ethanol (1:1) and 90-μl aliquots were injected on an Agilent 1100 HPLC equipped with a Merck LiChrospher column (250 mm × 4.6 mm) and packed with 100 RP-18 (5 μm). The column was eluted at a flow of 0.75 ml min^{-1}; eluted peaks were detected by a diode array detector. After injection of the sample, the column was washed for 5 min with 50% ethanol in methanol (v:v), eluted with a linear gradient of 50% to 100% ethanol in 10 min, followed by 10 min isocratic washing with 100% ethanol. The main fraction eluting after 14.8 min (t_r = 14.8′) and showing a menaquinone-type UV spectrum was collected for further analyses (Supporting information, Fig. S5). This fraction and references were evaporated to dryness with a rotary vacuum film evaporator (BÜCHI Labortechnik AG, Switzerland) and dissolved in dichloromethane. Hereafter, samples were analyzed on an AccuTOF CS JMS-T100CS mass spectrometer (JEOL Ltd., Japan) equipped with a direct inlet probe and using methane for chemical ionization.

2.6. Bioinformatics tools

Genome (PRJNA16685), transcriptome (GSE15408) and whole-cell proteome data (PSE111) of *K. stuttgartiensis* were obtained from previous work [16,25] and are available from publicly available databases. Gene expression data, reported as RPKM (reads per kilobase per million) values, were considered to be significant if they exceeded a stringent value of 12.88, which corresponded to one-fold coverage of a gene of average length of 780 bp and 75 bp transcription reads. All transcribed and translated ORFs were re-evaluated for the presence of an N-terminal signal sequences and for the presence and number of transmembrane-spanning helices (TMH) using the SignalP 4.1 [56] and TMHMM 2.0 [57] software packages, respectively. All proteins discussed in this paper were assessed against validated proteins by multiple protein sequence alignments using the ClustalW program [58]. Abundant proteins in the membrane proteome that had been annotated at the time of the deposition of the genome [16] as 'hypothetical' or as 'unknown' were reconsidered for a putative function employing BLAST searches, COG and PFAM databases, as well as by applying the HHpred homology detection and structure prediction program [59].

3. Results

3.1. The membrane proteome of Kuenenia stuttgartiensis

First, we established the protocol outlined in the Materials and Methods section for the reproducible dissolving of integral RCs from membrane preparations of *K. stuttgartiensis*, their separation and molecular mass estimation by BNE, and their identification by proteomics (Supporting information, Figs. S1 and S2). The highly abundant heterotrimeric HZS [25,27] and the most abundant ATPase (H^+-dependent F_1F_O-ATPase; *K. stuttgartiensis* identification numbers kuste3787–3796) [60] were used for the validation of correct complexome profiling (Supporting information, Fig. S3C). It should be noted that the cell biology of anammox bacteria is rather complicated. The cells are bounded by three membrane layers, representing the periplasmic and cytoplasmic membranes like in Gram-negative bacteria, and the membrane surrounding the anammoxosome [31,32,49,61]. Since whole cells were used in membrane preparation, protein complexes present in each of the three membrane systems were recovered.

Once optimized, we applied the protocol to two BNE gradient gels, 4–16% and 3–12% polyacrylamide, which were cut in 65 and 66 equally sized pieces, respectively. Next, these 131 gel slices were subjected to shotgun proteomics, yielding a total of 1391 unambiguously identified proteins (Table 1, Supporting information Table S1). These included proteins that would be putatively soluble proteins (919) because of

Table 1
Overview of transcribed genes and detected proteins. Transcription values [16,25] were considered to be significant if they exceeded an RPKM ≥ 12.88 as explained in Materials and methods Section 2.6.

# of genes	Total encoded in the genome	Transcribed	Detected in at least one BN gel	Detected, but not transcribed	% detected of transcribed
Genome	4663	4060	1354	37	33.3
0 TMH	3582	3096	894	25	28.9
1 TMH	609	507	225	6	44.4[a]
≥2 TMH	472	457	235	6	51.4

[a] This value could be an underestimation, since a single TMH might represent a signal peptide with N-terminal cleavage site, making the processed protein a soluble one after transport across a membrane. Prediction of signal peptides using the SignalP 4.0 program [56] was not straightforward, because anammox bacteria might not fit in the classification system used for prediction.

the lack of any (predicted) transmembrane helices (TMHs), as well as proteins that would be membrane-bound by the presence of one (231) or more (241) TMHs. Interestingly, we also found proteins that would not have been transcribed based on their expression values [16,25].

Based on their migration profiles across the gels only, co-migrating proteins were then hierarchically clustered, putatively representing protein complexes (Supporting information, Figs. S3A,B). In this way, well over a hundred of clusters were obtained that were related a range of biological functions such as transcription (RNA polymerase), translation (ribosomal proteins), signaling and regulation, cell division, protein repair (chaperone proteins), transport of polypeptides or small compounds across membranes, or lipid and cell wall metabolism (see f.i. Supporting information, Table S2). In our analysis we focused on protein systems that are of interest not only for the better understanding of anammox energy and carbon metabolism, but also from the general perspective of prokaryotic bioenergetics because of their wide-spread occurrence in bacterial genomes. The results of the in-depth analysis of seven protein systems displayed in Fig. 2 (HZS, NXR, Complex I, NQR, RNF and Complex III) and of the four ATPases coded by the genome of *K. stuttgartiensis* will be discussed hereafter.

3.2. Protein complexes of the anammox reactions

Enzymes involved in the anammox process (Fig. 1) are localized in the anammoxosome [40]. Despite being soluble enzymes, the two most highly expressed proteins (HDH and HZS) were easily detected even in carefully washed membrane preparations (Supporting information, Table S2). In contrast, nitrite reductase NirS, the proposed candidate nitrite reductase [16], was barely detectable, as expected from its low transcription levels [25]. Besides HDH [28], nine more HAO-like octaheme proteins encoded in the *K. stuttgartiensis* genome [16,25,26] were retrieved in the proteome (Supporting information, Table S2 and Fig. S3B) and one of these (kust4574) formed part of a novel Rieske/cyt*b* complex described later (Section 3.6). Importantly, the products of the hydrazine synthase (*hzs*) gene cluster (kuste2854–61; Supporting information, Fig. S4A) migrated into two distinct protein complexes as well as a low-molecular weight *c*-type triheme protein (kuste2854) (Fig. 2A). The first complex was the catalytic heterotrimeric HZS (kust2859–61) [25,27]. The second complex comprised the ETM (kuste2855–56) that was predicted from genome analyses [26]. These analyses suggested ETM to be a quinol-binding RC, embedded in the membrane by the presence of seven TMHs per heterodimer (Supporting information, Fig. S4A) [26]. In fact, ETM was observed as two bands migrating in the gels with apparent molecular masses of ~140 and ~300 kDa (Fig. 2A), indicative of $(\alpha\beta)_2$ and $(\alpha\beta)_4$ subunit compositions, respectively. HZS and ETM did not co-migrate as higher order aggregates. Neither did triheme kuste2854, the proposed electron shuttle between HZS and ETM [26], associate to any of the two; kuste2854 was mainly observed in the low-molecular mass gel slices

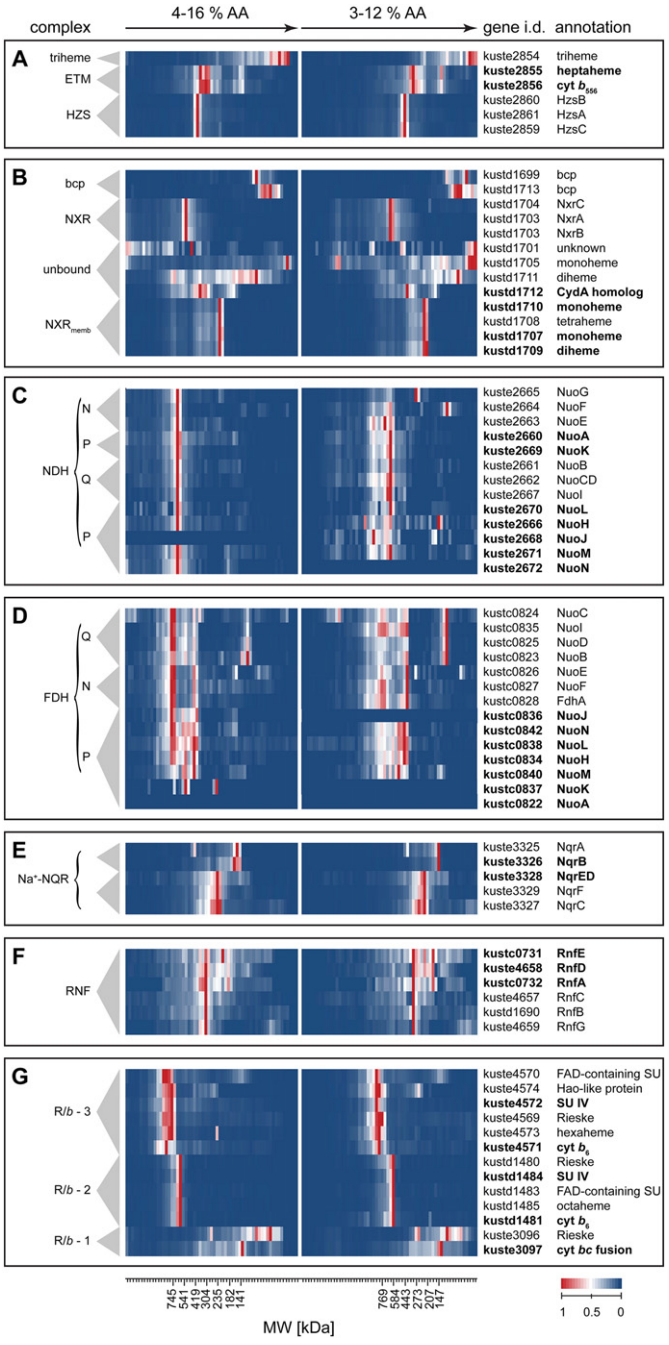

Fig. 2. Heat maps derived from hierarchical clustering of the protein migration profiles of seven protein systems described in the text. AA, acrylamide gradients; ETM, putative electron transfer module; HZS, hydrazine synthase; bcp, putative blue-copper containing protein; NXR, nitrite:nitrate oxidoreductase; unbound, proteins of the *nxr* gene cluster not forming a complex with other proteins; NXR$_{memb}$: proteins (kustc1707-10) of the *nxr* gene cluster present as an abundant membrane-bound complex; NDH, NADH dehydrogenase; FDH, putative membrane-bound formate dehydrogenase; N, catalytic electron input module facing the cytoplasm; P, the membrane-bound H^+-translocating module; Q, the connecting electron-transfer adapter module. Na^+-NQR, sodium-dependent NADH:quinone oxidoreductase; RNF, H^+/Na^+-translocating NAD^+:ferredoxin oxidoreductase; Rieske/cyt*b*: Rieske/cytochrome *b*-containing complex similar to the quinol:cytochrome *c* oxidoreductase (complex III). Proteins in bold contain at least 2 predicted TMHs.

(Fig. 2A). Unfortunately, examination of migration patterns did not reveal a candidate RC mediating hydrazine oxidation to the reduction of the Q-pool (Fig. 1). If existent, its component(s) were not amongst the 70 highest abundant proteins listed in Supporting information, Table S2. However, quinones could be readily extracted from the membranes,

and the major species was identified as menaquinone-7 (MK-7) (Supporting information, Fig. S5). In agreement herewith, MK-7 was the dominant quinone also in '*Candidatus* Jettenia caeni' [62].

3.3. Nitrite oxidation to nitrate

Nitrite oxidation to nitrate, catalyzed by NXR, replenishes the electrons that are withdrawn from the cyclic electron flow for CO_2 fixation. Previously, NXR was isolated as a soluble trimeric protein (molecular mass, ~215 kDa) encoded by kustd1700/03/04 and immunogold labelling showed its exclusive localization inside the anammoxosome [40]. The kustd1700/03/04 structural genes form part of the large *nxr* gene cluster (kustd1699–1713) that additionally encodes a series of *c*- and *b*-type hemes, and two putative BCPs, all with still unknown functions (Supporting information, Fig. S4B) [26]. Products of most of these *nxr* genes were recovered in our membrane proteome analyses (Figs. 2B and 3). More specifically, NXR migrated in the 4–16% and 3–12% gradient gels as a tight complex with apparent molecular masses of 510 and 625 kDa, respectively (Fig. 3B). The latter values are suggestive of a trimeric configuration. Next, a highly abundant protein cluster, tentatively called membrane-bound NXR cluster (NXR_{memb}), was identified that was composed of monoheme *c* protein kustd1707, tetraheme *c* protein kustd1708, diheme *b* protein kustd1709 and monoheme *c* kustc1710 (Fig. 3D). As judged from the migration distances, this complex was predominantly present having an apparent molecular mass of ~200 kDa; minor amounts were observed at ~330 kDa. These values were higher than expected for a kustc1707/08/09/10 complex being assembled in an $(\alpha\beta\gamma\delta)_1$ configuration (160 kDa). The presence of six TMHs would make NXR_{memb} membrane-bound (Supporting information, Fig. S4B). Another membrane protein was represented by kustd1712 (16 TMHs) (Fig. 3C). Interestingly, kustd1712 has appreciable sequence homology [20,26] to the quinol-binding CydA subunit of a cytochrome *bd* terminal oxidase [63,64]. We found no evidence for an association between kustc1712 and NXR_{memb}. Neither did the remainder of the observed *nxr* gene products associate with other components; they were detected in low-molecular range gel slices only (Fig. 3C), suggesting a role as mobile electron carriers.

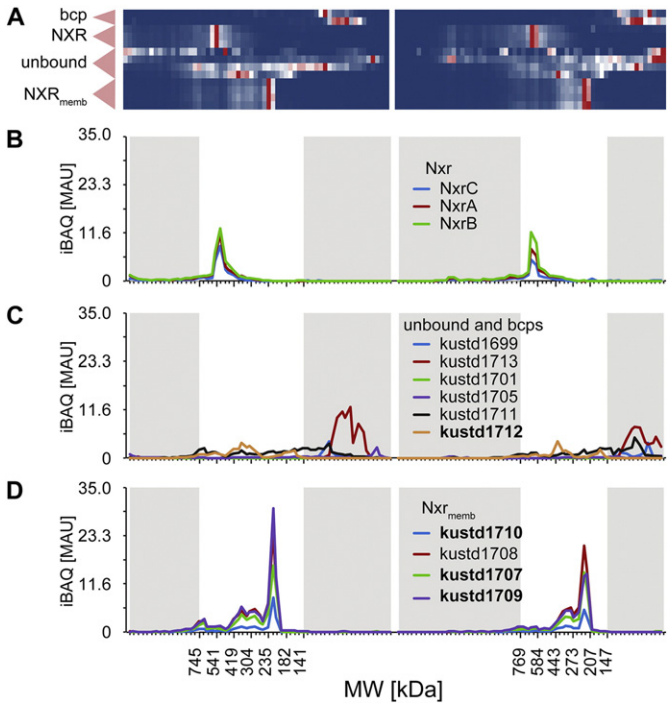

Fig. 3. Hierarchical clustering and protein migration profiles of the components of the nitrite:nitrate oxidoreductase (NXR) system from *K. stuttgartiensis*. A) Heat maps derived from hierarchical clustering of the protein migration profiles and ordered according their putative functions. Bcp, blue copper proteins (kustd1699 and kustd1713); NXR, catalytic complex represented by the NxrA (kustd1700), NxrB (kustd1703) and NxrC (kustd1704) subunits; unbound, proteins that do not form part of a higher-order complex (see also Fig. 3C); NXR_{memb}, membrane-bound complex. B) Protein migration profiles of the NxrABC subunits. C) Protein migration profiles of the bcps and other proteins encoded in the *nxr* gene cluster not forming part of the detected (sub)complexes. D) Protein migration profiles of each subunit of the novel membrane-bound complex. Protein migration profiles were visualized by plotting the protein abundance (iBAQ) values of each identified polypeptide against the calculated molecular weight. Areas outside the linear molecular weight range are shaded grey. Proteins in bold contain at least 2 predicted TMHs.

3.4. NAD(P)H:quinone oxidoreductases

Quinone reduction by NADH is catalyzed by two genetically unrelated RCs: a proton-pumping enzyme (NDH-1, NUO, Complex I) and an enzyme that uses Na^+ as coupling ion (Na^+-NQR). Whereas NUO is ubiquitously found in bacteria, the presence of NQR is restricted to marine and pathogenic microorganisms [65]. Remarkably, the genome of *K. stuttgartiensis* encodes both types [16,25] and intriguingly, complexome profiling showed the expression and assembly of both complexes (Fig. 2C and E). NDH-1, which contains 13 subunits in prokaryotes, can be thought to be composed of three modules: an electron input (N-) module facing the cytoplasm, a connecting electron transfer (Q-) module and the membrane-bound H^+-translocating (P-) module [66]. The integral complex is not commonly detected in gel-based proteomics and disintegrates easily. However, here hierarchical clustering immediately identified a protein complex with a size of ~620 kDa in both gels that harbored all subunits of *K. stuttgartiensis* NDH-1 (kuste2660–72; theoretical mass, 575 kDa) (Figs. 2C and 4A,B). In the 4–16% gradient gel, all subunits comigrated as a tight band, except for the subunit NuoJ (kuste2668, 21.0 kDa, 3 TMHs), which was not detected. However, the latter was observed in the 3–12% gradient gel, where the NDH-1 band was more diffuse and where NuoN (kuste2672, 52.9 kDa, 14 TMHs) remained beyond detection. In this 3–12% gel, the N-module NuoG (kuste2665) and NuoF (kuste2664) subunits were also detected on their own, presumably as the result of a partial disintegration of the Nuo complex under this chromatographic condition, leaving the P- and Q-module subunits as a subcomplex.

The modular organization of NDH-1 is evolutionarily conserved in other enzymes that notably differ in the composition of the N-input module, lending these different functionalities [66–68]. The genome of *K. stuttgartiensis* codes for two of these and both were found in our proteomic analysis. The first enzyme was encoded by the kustc0822–42 gene cluster (Supporting information, Fig. S4C). The presence of an additional gene coding for the formate dehydrogenase catalytic subunit (FdhA) suggested the complex to act as a membrane–bound formate dehydrogenase (FDH) probably catalyzing CO_2 reduction for acetyl-CoA synthesis. The second enzyme could represent an unknown type of hydrogenase (Supporting information, Fig. S6). Even though all predicted FDH subunits, except the hydrophobic subunit NuoA, (kustc0822; 13.5 kDa, 3 THMs) were recovered, migration patterns were somewhat diffuse, especially in the 3–12% gradient gel (Figs. 2D and 4A,C). In the 4–16% BNE gel, two high-molecular complexes of ~750 kDa and ~500 kDa could be clustered that comprised most of the FDH subunits. The mass of the smaller complex (~500 kDa) favorably corresponds to the theoretical mass of FDH (540 kDa). It is, however, unknown, what determined the increased mass of the larger complex (~750 kDa). Next, a subcomplex was observed at ~400 kDa composed of the P- and Q-modules, thus lacking the input (N-) module (expected, 360 kDa), whereas the Q-module only ((NuoBCDI; kustc0824–26, kustc0835) also migrated as a distinct band (observed, 100 kDa; expected 97 kDa). This view, albeit somewhat more diffuse, was supported by the 3–12% gradient gel (Fig. 4AC, right panels). Apparently, the FDH complex is refractory towards BNE, at which it disintegrates into a number of subcomplexes.

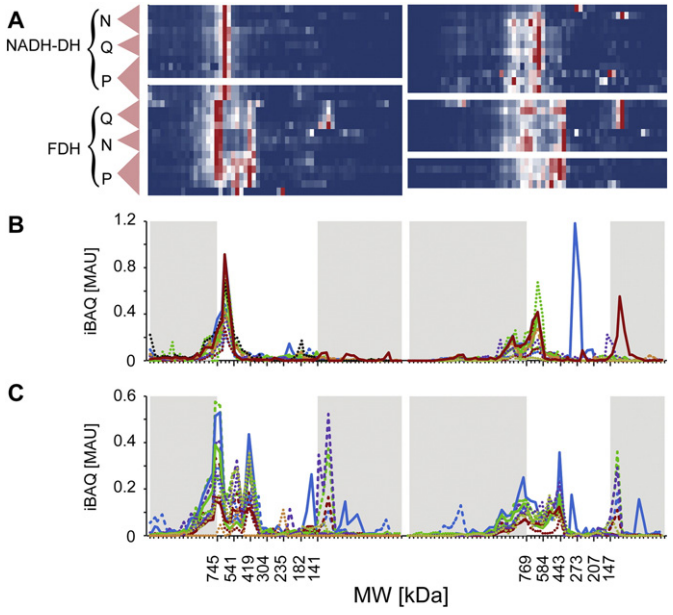

Fig. 4. Hierarchical clustering and protein migration profiles of the NADH:quinone oxidoreductase (NADH-DH, complex I) and formate dehydrogenase (FDH) systems from *K. stuttgartiensis*. A) Heat maps derived from hierarchical clustering of the protein profiles of the NADH-DH and FDH systems. N (electron input), Q (connecting electron transfer), and P (membrane-bound proton translocation) refer to the modular organizations of these complexes. B) Protein migration profiles of each subunit of the NADH-DH complex. C) Protein migration profiles of each subunit of the FDH complex. In vertical order, heat maps of the individual subunits (Fig. 4A) and their migration profiles presented in different line styles and line colors (Fig. 4B,C) are the following: **NADH-DH** N module (solid lines), NuoG (kuste2665; blue), NuoF (kuste2664; red), NuoE (kuste2663; green); Q module (dashed lines), NuoB (kuste2661; blue), NuoCD (kuste2662; red), NuoI (kuste2667; orange); P module (dotted lines), NuoA (kuste2660; orange), NuoK (kuste2669; blue), NuoL (kuste2670; red), NuoH (kuste2666; green); NuoJ (kuste2668; yellow); NuoN (kuste2672; black); NuoM (kuste2671; purple). **FDH** Q module (dashed lines), NuoC (kustc0824; blue), NuoI (kustc0835; red), NuoD (kustc0825; green), NuoB (kustc0823; purple); N module (solid lines), NuoE (kustc0826; blue), NuoF (kustc0827; red), FdhA (kustc0828; green); P module (dotted lines), NuoJ (kustc0836; blue), NuoN (kustc0842; purple), NuoL (kustc0838; green), NuoH (kustc0834; red), NuoM (kustc0837; yellow), NuoK (kustc0837; orange). Protein migration profiles were visualized by plotting the protein abundance (iBAQ) values of each identified subunit against the calculated molecular weight. Areas outside the linear molecular weight range are shaded grey.

Na^+-NQR is encoded by the gene cluster kuste3329–33 (*nqr*A–F; subunits D and E are fused, which is uncommon). Although all subunits were detected in both BNE gradient gels, they migrated as two tight subcomplexes comprising NqrAB (observed, ~150 kDa) and NqrCDEF (observed, ~230 kDa) (Fig. 2E). The apparent molecular masses were approximately two-fold higher than predicted (NqrAB, 80 kDa; NqrCDEF, 139 kDa), indicating that both subcomplexes were present as dimers, which has not been reported for this enzyme [65,69].

3.5. Generation of reduced ferredoxin

Several carbonylation reactions in CO_2 fixation including its key reaction, acetyl-CoA synthesis, depend on the reducing power of reduced ferredoxin (Fd_{red}). Thus far, it was unknown how Fd_{red} would be generated in anammox bacteria. Our proteome analysis offered a likely candidate in an unexpected way: Na^+ (or H^+)-translocating NAD^+:ferredoxin oxidoreductase (RnfABCDEG) (reviewed in [65,70]). This particular complex migrated to a molecular mass of ~320 kDa (Fig. 2F). Its six subunits could be identified as the gene products of kustc0731 and kustc0732, which had been erroneously annotated as two NqrDE homologs (NqrDE and RnfEA sequences are highly similar [65]), RnfCDG (kust4657–59), and RnfB (kustd1690). Thus, besides erroneous annotations, the encoding genes were spread across the genome, which was highly likely the reason why the complex had previously been overlooked. Next to the 320 kDa holocomplex, a subcomplex was detected in both gels, migrating at approximately 180 kDa and containing the membrane-bound subunits RnfEAD only. One may note that the estimated molecular masses both were about twice the theoretical values of monomeric RnfABCDEF (187 kDa) and monomeric RnfEAD (83 kDa), indicating the holo- and sub-complexes to migrate as dimers.

3.6. All three Rieske/cytb complexes found in the genome in of K. stuttgartiensis are expressed

The genome of *K. stuttgartiensis* harbors the genetic information for three putative Rieske/cyt*b* complexes, encoded by kuste3096–97 (R/*b*-1), kustd1480–1485 (R/*b*-2) and kuste4569–4574 (R/*b*-3) (Supporting information, Fig. S4D) [16,25,26]. All three contain the core components of canonical Rieske/cyt*b* complexes: the Rieske-type iron-sulfur protein, a membrane-bound heme *b* subunit and a *c*-type heme subunit. However, all three gene clusters show variations on this common theme: R/*b*-1 encodes a fusion protein of the *b*- and *c*-type hemes, while in R/*b*-2 and R/*b*-3 the heme *b* subunit is split like in the b_6f complexes of photosynthetic organisms and *Firmicutes*. Specific genes in these two operons include multiheme *c* proteins (octaheme kustd1483 and hexaheme kuste4573), putative FAD-dependent subunits of an $NAD(P)^+$ oxidoreductase (kustd1483 and kuste4570) and an HAO-like octaheme-containing protein (encoded by kuste4574 in R/*b*-3 only) [20,26].

Our proteomic data revealed that all subunits of the three Rieske/cyt*b* complexes were expressed at the protein level (Figs. 2G and 5). The two gene products of R/*b*-1 were the least abundant and did not co-migrate as one complex (Fig. 5D). In contrast, all gene

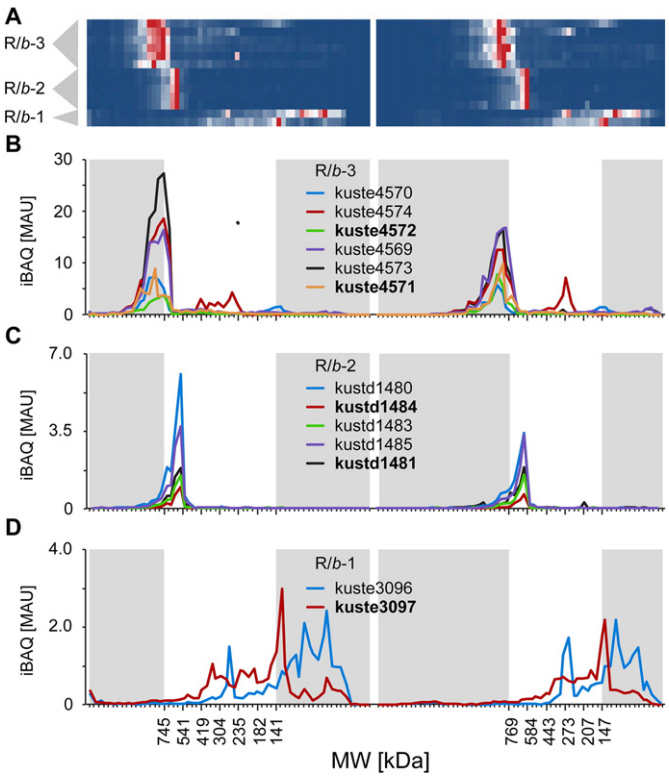

Fig. 5. Hierarchical clustering and protein migration profiles of the three Rieske/cyt*b* complexes from *K. stuttgartiensis*. A) Hierarchical clustering was based on relative abundances. The vertical order of the subunits is as specified in Fig. 5,B–D). B–D) Protein migration profiles of the individual subunits of the three Rieske/cyt*b* complexes. Migration profiles were visualized by plotting the protein abundance (iBAQ) values of each identified subunit against the measured molecular weight. Areas outside the linear molecular weight range are shaded grey. Proteins in bold contain at least 2 predicted TMHs.

products of R/*b*-2 and R/*b*-3 clearly co-migrated as sharply focused protein complexes, which included the additional gene products mentioned. R/*b*-3 was the most abundant Rieske/cyt*b* complex in the membrane preparations. Migration sizes of approximately 580 kDa and 860 kDa of R/*b*-2 and R/*b*-3, respectively, showed these complexes to be present as dimers, as is commonly the case for Rieske/cyt*b* complexes. Importantly, no subcomplexes lacking either the NAD(P)$^+$ oxidoreductase, multiheme or HAO-like subunits could be detected. However, part of the HAO-like protein migrated as a homotrimer at ~250 kDa.

3.7. ATP synthesis is catalyzed by ATPase-1

The genome of *K. stuttgartiensis* encodes four different membrane-bound ATPases: The ubiquitous H$^+$-dependent F_1F_O-type (ATPase1, kuste3787–3796) and two types (ATPase-2, kuste4592–4600; ATPase-3; kustc0572–0579) that lack the δ subunit, but contain one or two additional membrane subunits (AtpQ, kuste4594 and kustc0574; AtpR, kuste4595) instead (Supporting information, Fig. S4E) [16,26,60]. The latter two ATPases have been suggested to act as Na$^+$-pumping ATP hydrolases (N-ATPase) [71]. Besides these, a prokaryotic V-type ATPase is encoded (ATPase-4, kuste3864–3871).

The migration profiles of the ATPases presented here fully supported previous studies that suggested ATPase-1 to be the main ATP synthase in *K. stuttgartiensis* [59] (Fig. 6). All detected subunits migrated in both gradient gels as a narrow band to a molecular mass of ~620 kDa. However, neither the water-insoluble small rotor ring subunit c (AtpE, kuste3790), the small AtpI subunit (kustc3787; 9.2 kDa), nor the b (AtpF, kuste3791) and δ (AtpH, kuste3792) subunits were found, the latter two because of annotation errors in the genome database [60]. Considering the calculated molecular mass of the complete ATP synthase (550 kDa), the 620 kDa band still might contain the complete F_1F_O complex. A minor amount of the soluble $\alpha_3\beta_3$ F_1 subcomplex could also be detected in a peak at ~440 kDa (Fig. 6). This Figure also shows the migration profiles of the other three ATPases. Although not as distinct as for ATPase-1, most subunits of the N- and V-ATPases were recovered as high-molecular mass complexes and subcomplexes, but their expression was considerably lower than that of ATPase-1. It should be noted that the existence of N-ATPases was only predicted from genomic analyses [71], but their expression at the protein level had never been demonstrated thus far.

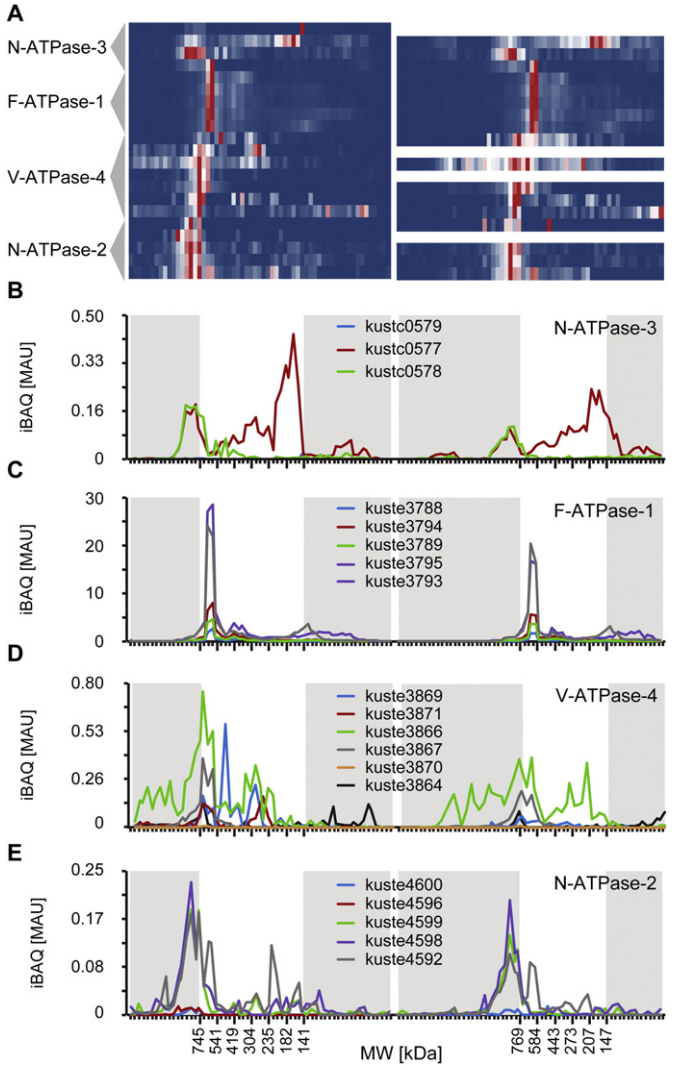

Fig. 6. Identification by complexome profiling the four ATPase complexes from *K. stuttgartiensis*. A) Hierarchical clustering of relative abundances of identified proteins in each gel slice. In blank rows, gene products were not detected. The vertical order of the gene products is as specified in panels B–E. B–E) Absolute abundances (iBAQ values, Arbitrary Units) of each subunit. Abundances were plotted against the apparent molecular masses in the BN gels. The subunits of the F-ATPase-1 were mainly detected at molecular weights corresponding to the whole F_1-F_O ATP synthase complex (550 kDa). The absolute abundance of each complex confirmed F-ATPase-1 as the most abundant in the membranes. Areas outside the linear molecular weight range are shaded grey.

4. Discussion

Complexome profiling presented a very suitable tool for the comprehensive analysis of respiratory protein complexes in *K. stuttgartiensis*. This method verified the presence of not only nearly all RCs but also other protein complexes that had been predicted from genomic analyses [26] and results, such as the composition of the HZS [27] and NXR proteins [39,40], were in full agreement with still scarce experimental evidence. The method showed how gene products of long gene clusters assembled as distinct protein complexes that are known from other organisms (complex I, ATP synthase) or that are typical for anammox bacteria, such as the *hzs* and *nxr* systems for which the assembly of the hypothetical ETM and NXR_{memb} complex, respectively, could be shown (Fig. 2 and Fig. 3; Supporting information, Fig. 4). The method even allowed the detection of an RC, NAD$^+$:ferredoxin oxidoreductase (RNF), composed of subunits encoded by genes that are spread over the genome. On top of this, results obtained by complexome profiling changed our view on anammox energy metabolism in at least two ways (Fig. 7).

Complexome profiling has proven its strength in OXPHOS research [42–46] and provided us with a very fruitful method to analyze the membrane proteome of anammox bacteria. However, the method has some limitations. Firstly, not all subunits of every RC could be detected in all cases. Reliable proteomic identification and quantification of a protein depends on the absolute protein amount and the presence of a sufficient number of detectable peptides by MS after protein digest. Furthermore, peptides might be undetectable if they are too small (<6 amino acids), when they poorly fragment (structural properties), or when they are too hydrophilic or too hydrophobic. These limitations especially apply to membrane proteins that may be poorly soluble, can be small and/or lack sites that are subject to proteolytic cleavage [72,73]. Nevertheless, membrane proteins were recovered with appreciable efficiency, also hydrophobic ones with multiple TMHs (Table 1). Secondly, molecular mass estimations based on migration in the BNE gels were not always in agreement with calculated ones or with values determined for known isolated protein complexes. This could be expected, since electrophoretic behavior of a protein (complex) may be affected by the presence of lipids and detergents, and its size, shape and compactness [48,50]. Moreover, several protein complexes apparently migrated as dimers or even multimers. Presently it is unknown whether such migration is an aggregation artifact caused by BNE conditions or reflects a physiological state. Nevertheless, the migration as dimers (or multimers) implies that the pertinent complexes can interact and

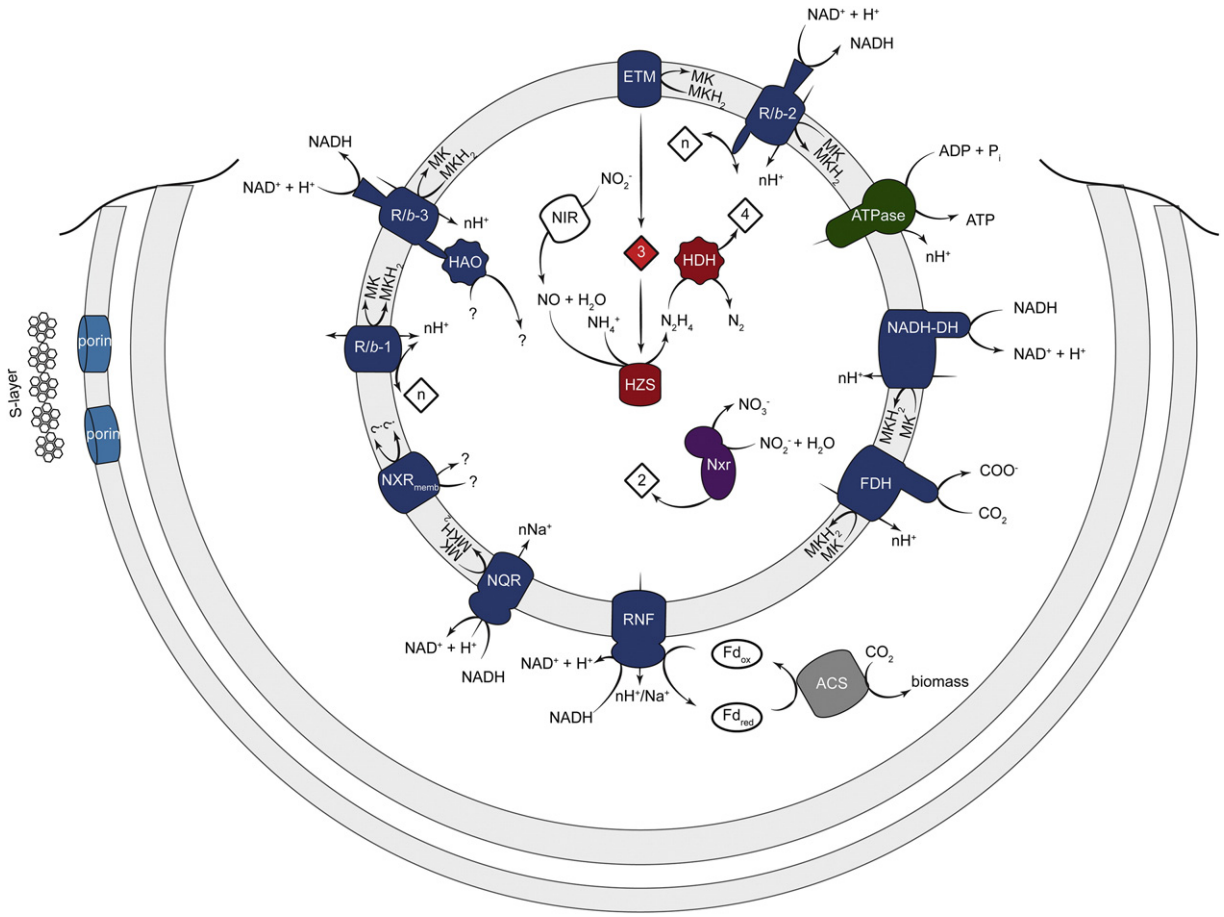

Fig. 7. Proteome-based revised overview of processes involved in the anammox reactions, ATP synthesis and carbon fixation in *K. stuttgartiensis*. The grey concentric circles represent the three (periplasmic, cytoplasmic) membrane systems that surround the anammox cell with the anammoxosome membrane in the center. The highly abundant S-layer [49] and porin proteins [85] that were present in the membrane preparations are localized in the outer aspects of the cell. ACS, acetyl-CoA synthase/CO dehydrogenase representing carbon fixation by the reductive acetyl-CoA pathway (please, note that ACS itself, being a soluble protein, was not addressed in this study); ATPase, ATP synthase; ETM, electron transfer module from the Q-pool to HZS; FDH, putative membrane-bound formate dehydrogenase/CO_2 reductase; HDH, hydrazine dehydrogenase; HZS, hydrazine synthase; NADH-DH, NADH dehydrogenase; Nir, nitrite reductase; NXR, nitrite:nitrate oxidoreductase; NXR_{memb}, membrane-bound complex of the *nxr* gene cluster. R/*b*: Rieske/cytochrome *b* complexes. White shapes indicate proteins with no identified gene candidate. Diamonds indicate putative cytochrome *c*-type proteins with the number of electrons that are transferred.

associate. Such association could be of physiological relevance, indeed, as exemplified for instance by the dimeric ATPase and respiratory supercomplexes in mitochondria and bacteria [74–77].

A still open question in our understanding of anammox energy metabolism is how the energy obtained from hydrazine oxidation, which is nature's most powerful reductant ($E_m' = -0{,}75$ V), is conserved into an electrochemical gradient. In analogy with other prokaryotic electron transfer systems [78], it was hypothesized that this could be achieved by the action of a quinone-reducing RC (Fig. 1) [26], but we could not find any evidence for the presence of such a protein (complex). Although the presence, albeit in low amounts, of this hypothetical protein that would lack any similarity to known quinone-reducing RCs still cannot be ruled out, our results suggested an intriguing alternative: the unusual Rieske/cyt*b* RCs (Figs. 5 and 7). By accepting the electrons from hydrazine oxidation, energy would be conserved as NAD(P)H, reduced quinone, in this case menaquinol-7, and perhaps also as a *pmf*. However intricate, this set of reactions is thermodynamically feasible and the unusual Rieske/cyt*b* RCs do harbor the components to carry out this complex process. The presence of the HAO-like protein in the most abundant R/*b*-3 could even account for the as yet elusive nitrite reductase. Hereby, the novel Rieske/cyt*b* RCs would be central in anammox energy metabolism, as are related b_6f complexes in photosynthetic organisms [79–83].

In agreement with previous studies [60], H^+-pumping F_1F_O-ATPase was found to be the major ATPase (Fig. 6), implying that anammox bacteria thrive on a *pmf* most likely across the anammoxosome membrane. An unexpected result of this study was that *K. stuttgartiensis* expresses and assembles a set of RCs that use Na^+ as the coupling ion, suggesting that the organism utilizes a sodium-motive force (*smf*) as well. This *smf* could be established by the action of Na^+-NQR (Figs. 2E and 7), and possibly of the sodium-pumping N-ATPases. Next, this *smf* would support the thermodynamically unfavorable reduction of ferredoxin for cell carbon metabolism, catalyzed by the RNF complex detected here.

By our complexome analysis, we could confirm the presence of a range of respiratory complexes in *K. stuttgartiensis* for the first time, the existence of which was predicted from genomic analyses [26]. It should be stressed that all of these complexes are not unique for this particular anammox species, but are conserved in all anammox genomes sequenced to date. In fact, genes coding for several of these novel complexes are found in genomes of other ecologically relevant microorganisms as well. For instance, BLAST searches immediately reveal NXR_{memb} complex and *cyd*A homologs in nitrite oxidizers, certain sulfate reducers, magnetotactic bacteria and giant *Thiomargarita* species. The unusual Rieske/cyt*b* RCs characterized by the presence of NAD(P)-reducing and multiheme subunits are found in a variety of species, and even form a separate clade within the rapidly expanding class of complex III RCs [80,84]. Taken together, our results expand our knowledge of the still poorly understood versatility of prokaryotic respiratory systems. Our findings were achieved by the application of

complexome profiling, which we believe has a general applicability in concert with (meta)genomics, allowing the sensitive detection and validation of the huge variety of novel RCs predicted from genomic analyses.

Transparency document

The Transparency document associated with this article can be found, in online version.

Acknowledgements

This work was supported by the Netherlands Organization for Scientific Research (NWO) by ALW grant ALW2PJ/08021 (to N.M.dA) and VENI grant 863.11.003 (to B.K.), by the European Research Council, Starting Grant number ERC 640422 (to B.K) and Advanced Grants numbers ERC 232937 and ERC 339880 (to M.S.M.J.).

Appendix A. Supplementary data

Supplementary data to this article can be found online at http://dx.doi.org/10.1016/j.bbabio.2016.07.006.

References

[1] P. Mitchell, Chemiosmotic coupling in oxidative and photosynthetic phosphorylation, Biol. Rev. Camb. Philos. Soc. 141 (1966) 445–502.
[2] B. Schoepp-Cothenet, R. van Lis, A. Atteia, F. Baymann, L. Capowiez, A.L. Ducluzeau, S. Duval, F. ten Brink, M.J. Russell, W. Nitschke, On the universal core of bioenergetics, Biochim. Biophys. Acta 1827 (2013) 79–93.
[3] M.S. Rappé, S.J. Giovannoni, The uncultured microbial majority, Annu. Rev. Microbiol. 57 (2003) 369–394.
[4] S.M. Sievert, K.M. Scott, M.G. Klotz, P.S. Chain, L.J. Hauser, J. Hemp, M. Hügler, M. Land, A. Lapidus, F.W. Larimer, S. Lucas, S.A. Malfatti, F. Meyer, I.T. Paulsen, Q. Ren, J. Simon, USF Genomics Class, Genome of the epsilonproteobacterial chemolithoautotroph *Sulfurimonas denitrificans*, Appl. Environ. Microbiol. 74 (2008) 1145–1156.
[5] Y. Liu, L.L. Beer, W.B. Whitman, Sulfur metabolism in archaea reveals novel processes, Environ. Microbiol. 14 (2012) 2632–2644.
[6] F. Grein, A.R. Ramos, S.S. Venceslau, I.A. Pereira, Unifying concepts in anaerobic respiration: insights from dissimilatory sulfur metabolism, Biochim. Biophys. Acta 1827 (2013) 145–160.
[7] K.M. Handley, D. Bartels, E.J. O'Loughlin, K.H. Williams, W.L. Trimble, K. Skinner, J.A. Gilbert, N. Desai, E.M. Glass, T. Paczian, A. Wilke, D. Antonopoulos, K.M. Kemner, F. Meyer, The complete genome sequence for putative H_2- and S-oxidizer *Candidatus* Sulfuricurvum sp., assembled de novo from an aquifer-derived metagenome, Environ. Microbiol. 16 (2014) 3443–3462.
[8] J. Hemp, R.B. Gennis, Diversity of the heme-copper superfamily in archaea: insights from genomics and structural modeling, Results Probl. Cell Differ. 45 (2008) 1–31.
[9] K.F. Ettwig, M.K. Butler, D. Le Paslier, E. Pelletier, S. Mangenot, M.M. Kuypers, F. Schreiber, B.E. Dutilh, J. Zedelius, D. de Beer, J. Gloerich, H.J. Wessels, T. van Alen, F. Luesken, M.L. Wu, K.T. van de Pas-Schoonen, H.J. Op den Camp, E.M. Janssen-Megens, K.J. Francoijs, H. Stunnenberg, J. Weissenbach, M.S. Jetten, M. Strous, Nitrite-driven anaerobic methane oxidation by oxygenic bacteria, Nature 464 (2010) 543–548.
[10] T. Tosha, Y. Shiro, Crystal structures of nitric oxide reductases provide key insights into functional conversion of respiratory enzymes, IUBMB Life 65 (2013) 217–226.
[11] M. Ilbert, V. Bonnefoy, Insight into the evolution of the iron oxidation pathways, Biochim. Biophys. Acta 1827 (2013) 161–175.
[12] T. Goris, T. Schubert, J. Gadkari, T. Wubet, M. Tarkka, F. Buscot, L. Adrian, G. Diekert, Insights into organohalide respiration and the versatile catabolism of *Sulfurospirillum multivorans* gained from comparative genomics and physiological studies, Environ. Microbiol. 16 (2014) 3562–3580.
[13] R.A. Lesniewski, S. Jain, K. Anantharaman, P.D. Schloss, G.J. Dick, The metatranscriptome of a deep-sea hydrothermal plume is dominated by water column methanotrophs and lithotrophs, ISME J. 6 (2012) 2257–2268.
[14] S. Lücker, M. Wagner, F. Maixner, E. Pelletier, H. Koch, B. Vacherie, T. Rattei, J.S. Damsté, E. Spieck, D. Le Paslier, H. Daims, A *Nitrospira* metagenome illuminates the physiology and evolution of globally important nitrite-oxidizing bacteria, Proc. Natl. Acad. Sci. U. S. A. 107 (2010) 13479–13484.
[15] C.B. Walker, J.R. de la Torre, M.G. Klotz, H. Urakawa, N. Pinel, D.J. Arp, C. Brochier-Armanet, P.S. Chain, P.P. Chan, A. Gollabgir, J. Hemp, M. Hügler, E.A. Karr, M. Könneke, M. Shin, T.J. Lawton, T. Lowe, W. Martens-Habbena, L.A. Sayavedra-Soto, D. Lang, S.M. Sievert, A.C. Rosenzweig, G. Manning, D.A. Stahl, *Nitrosopumilus maritimus* genome reveals unique mechanisms for nitrification and autotrophy in globally distributed marine crenarchaea, Proc. Natl. Acad. Sci. U. S. A. 107 (2010) 8818–8823.
[16] M. Strous, E. Pelletier, S. Mangenot, T. Rattei, A. Lehner, M.W. Taylor, M. Horn, H. Daims, D. Bartol-Mavel, P. Wincker, V. Barbe, N. Fonknechten, D. Vallenet, B. Segurens, C. Schenowitz-Truong, C. Médigue, A. Collingro, B. Snel, B.E. Dutilh, H.J. Op den Camp, C. van der Drift, I. Cirpus, K.T. van de Pas-Schoonen, H.R. Harhangi, L. van Niftrik, M. Schmid, J. Keltjens, J. van de Vossenberg, B. Kartal, H. Meier, D. Frishman, M.A. Huynen, H.W. Mewes, J. Weissenbach, M.S. Jetten, M. Wagner, D. Le Paslier, Deciphering the evolution and metabolism of an anammox bacterium from a community genome, Nature 440 (2006) 790–794.
[17] M.S.M. Jetten, I. Cirpus, B. Kartal, L. van Niftrik, K.T. van de Pas-Schoonen, O. Sliekers, S. Haaijer, W. van der Star, M. Schmid, J. van de Vossenberg, I. Schmidt, H.J. Harhangi, M. van Loosdrecht, G.J. Kuenen, H. Op den Camp, M. Strous, 10 years of research on the anaerobic oxidation of ammonium, Biochem. Soc. Trans. 33 (2005) (1994-2004) 119–123.
[18] A.A. Van de Graaf, A. Mulder, P. de Bruijn, M.S. Jetten, L.A. Robertson, J.G. Kuenen, Anaerobic oxidation of ammonium is a biologically mediated process, Appl. Environ. Microbiol. 61 (1995) 1246–1251.
[19] A. Mulder, A.A. Graaf, L.A. Robertson, J.G. Kuenen, Anaerobic ammonium oxidation discovered in a denitrifying fluidized bed reactor, FEMS Microbiol. Ecol. 16 (1995) 177–184.
[20] B. Kartal, L. van Niftrik, J.T. Keltjens, H.J. op den Camp, M.S.M. Jetten, Anammox–growth physiology, cell biology, and metabolism, Adv. Microb. Physiol. 60 (2012) 211–262.
[21] M. Oshiki, H. Satoh, S. Okabe, Ecology and physiology of anaerobic ammonium oxidizing (anammox) bacteria, Environ. Microbiol. (2015), http://dx.doi.org/10.1111/1462-2920.13134 (ahead of print).
[22] P. Lam, M.M. Kuypers, Microbial nitrogen cycling processes in oxygen minimum zones, Ann. Rev. Mar. Sci. 3 (2011) 317–345.
[23] A.H. Devol, Denitrification, anammox, and N_2 production in marine sediments, Ann. Rev. Mar. Sci. 7 (2015) 403–423.
[24] B. Kartal, J.G. Kuenen, M.C. van Loosdrecht, Engineering. Sewage treatment with anammox, Science 328 (2010) 702–703.
[25] B. Kartal, W.J. Maalcke, N.M. de Almeida, I. Cirpus, J. Gloerich, W. Geerts, H.J. Op den Camp, H.R. Harhangi, E.M. Janssen-Megens, K.J. Francoijs, H.G. Stunnenberg, J.T. Keltjens, M.S. Jetten, M. Strous, Molecular mechanism of anaerobic ammonium oxidation, Nature 479 (2011) 127–130.
[26] B. Kartal, N.M. de Almeida, W.J. Maalcke, H.J. Op den Camp, M.S. Jetten, J.T. Keltjens, How to make a living from anaerobic ammonium oxidation, FEMS Microbiol. Rev. 37 (2013) 428–461.
[27] A. Dietl, C. Ferousi, W.J. Maalcke, A. Menzel, S. de Vries, J.T. Keltjens, M.S. Jetten, B. Kartal, T.R. Barends, The inner workings of the hydrazine synthase multiprotein complex, Nature 527 (2015) 394–397.
[28] W.J. Maalcke, J. Reimann, S. de Vries, J.N. Butt, A. Dietl, N. Kip, U. Mersdorf, T.R. Barends, M.S. Jetten, J.T. Keltjens, B. Kartal, Characterization of anammox hydrazine dehydrogenase, a key N_2-producing enzyme in the global nitrogen cycle, J. Biol. Chem. (2016), http://dx.doi.org/10.1074/jbc.M116.735530 (pii: jbc.M116.735530).
[29] A.B. Hooper, T. Vannelli, D.J. Bergmann, D.M. Arciero, Enzymology of the oxidation of ammonia to nitrite by bacteria, Antonie Van Leeuwenhoek 71 (1997) 59–67.
[30] P. Cedervall, A.B. Hooper, C.M. Wilmot, Structural studies of hydroxylamine oxidoreductase reveal a unique heme cofactor and a previously unidentified interaction partner, Biochemistry 52 (2013) 6211–6218.
[31] L. van Niftrik, W.J. Geerts, E.G. van Donselaar, B.M. Humbel, A. Yakushevska, A.J. Verkleij, M.S. Jetten, M. Strous, Combined structural and chemical analysis of the anammoxosome: a membrane-bounded intracytoplasmic compartment in anammox bacteria, J. Struct. Biol. 161 (2008) 401–410.
[32] L. van Niftrik, M.S.M. Jetten, Anaerobic ammonium-oxidizing bacteria: unique microorganisms with exceptional properties, Microbiol. Mol. Biol. Rev. 76 (2012) 585–596.
[33] F. Gori, S.G. Tringe, B. Kartal, E. Marchiori, M.S.M. Jetten, The metagenomic basis of anammox metabolism in *Candidatus* 'Brocadia fulgida', Biochem. Soc. Trans. 39 (2011) 1799–1804.
[34] J. van de Vossenberg, D. Woebken, W.J. Maalcke, H.J. Wessels, B.E. Dutilh, B. Kartal, E.M. Janssen-Megens, G. Roeselers, J. Yan, D. Speth, J. Gloerich, W. Geerts, E. van der Biezen, W. Pluk, K.J. Francoijs, L. Russ, P. Lam, S.A. Malfatti, S.G. Tringe, S.C. Haaijer, H.J. Op den Camp, H.G. Stunnenberg, R. Amann, M.M. Kuypers, M.S. Jetten, The metagenome of the marine anammox bacterium 'Candidatus Scalindua profunda' illustrates the versatility of this globally important nitrogen cycle bacterium, Environ. Microbiol. 15 (2013) 1275–1289.
[35] D. Hira, H. Toh, C.T. Migita, H. Okubo, T. Nishiyama, M. Hattori, K. Furukawa, T. Fujii, Anammox organism KSU-1 expresses a NirK-type copper-containing nitrite reductase instead of a NirS-type with cytochrome cd_1, FEBS Lett. 586 (2012) 1658–1663.
[36] Z. Hu, D.R. Speth, K.J. Francoijs, Z.X. Quan, M.S.M. Jetten, Metagenome analysis of a complex community reveals the metabolic blueprint of Anammox bacterium "*Candidatus* Jettenia asiatica", Front. Microbiol. 3 (2012) 366.
[37] D.R. Speth, L. Russ, B. Kartal, H.J. Op den Camp, B.E. Dutilh, M.S. Jetten, Draft genome sequence of Anammox bacterium "*Candidatus* Scalindua brodae," obtained using differential coverage binning of sequencing data from two reactor enrichments, Genome Announc. 3 (2015) (pii: e01415–14).
[38] M. Oshiki, K. Shinyako-Hata, H. Satoh, S. Okabe, Draft genome sequence of an anaerobic ammonium-oxidizing bacterium, "*Candidatus* Brocadia sinica", Genome Announc. 3 (2015) (pii: e00267–15).
[39] N.M. de Almeida, W.J. Maalcke, J.T. Keltjens, M.S.M. Jetten, B. Kartal, Proteins and protein complexes involved in the biochemical reactions of anaerobic ammonium-oxidizing bacteria, Biochem. Soc. Trans. 39 (2011) 303–308.
[40] N.M. de Almeida, S. Neumann, R.J. Mesman, C. Ferousi, J.T. Keltjens, M.S. Jetten, B. Kartal, L. van Niftrik, Immunogold localization of key metabolic enzymes in the anammoxosome and on the tubule-like structures of *Kuenenia stuttgartiensis*, J. Bacteriol. 197 (2015) 2432–2441.
[41] M. Strous, J.J. Heijnen, J.G. Kuenen, M.S.M. Jetten, The sequencing batch reactor as a powerful tool for the study of slowly growing anaerobic ammonium-oxidizing microorganisms, Appl. Microbiol. Biotechnol. 50 (1998) 589–596.

[42] H. Giese, J. Ackermann, H. Heide, L. Bleier, S. Dröse, I. Wittig, U. Brandt, I. Koch, NOVA: a software to analyze complexome profiling data, Bioinformatics 31 (2015) 440–441.
[43] H. Heide, L. Bleier, M. Steger, J. Ackermann, S. Dröse, B. Schwamb, M. Zörnig, A.S. Reichert, I. Koch, I. Wittig, U. Brandt, Complexome profiling identifies TMEM126B as a component of the mitochondrial complex I assembly complex, Cell Metab. 16 (2012) 538–549.
[44] T.A. Weber, S. Koob, H. Heide, I. Wittig, B. Head, A. van der Bliek, U. Brandt, M. Mittelbronn, A.S. Reichert, APOOL is a cardiolipin-binding constituent of the Mitofilin/MINOS protein complex determining cristae morphology in mammalian mitochondria, PLoS One 8 (2013) e63683.
[45] K. Kmita, C. Wirth, J. Warnau, S. Guerrero-Castillo, C. Hunte, G. Hummer, V.R. Kaila, K. Zwicker, U. Brandt, V. Zickermann, Accessory NUMM (NDUFS6) subunit harbors a Zn-binding site and is essential for biogenesis of mitochondrial complex I, Proc. Natl. Acad. Sci. U. S. A. 112 (2015) 5685–5690.
[46] C.S. Müller, W. Bildl, A. Haupt, L. Ellenrieder, T. Becker, C. Hunte, B. Fakler, U. Schulte, Cryo-slicing blue native-mass spectrometry (csBN-MS), a novel technology for high resolution complexome profiling, Mol. Cell. Proteomics 15 (2016) 669–681.
[47] L. Wöhlbrand, H.S. Ruppersberg, C. Feenders, B. Blasius, H.P. Braun, R. Rabus, Analysis of membrane-protein complexes of the marine sulfate reducer *Desulfobacula toluolica* Tol2 by 1D blue native-PAGE complexome profiling and 2D blue native-/SDS-PAGE, Proteomics 16 (2016) 973–988.
[48] I. Wittig, H.P. Braun, H. Schägger, Blue native PAGE, Nat. Protoc. 1 (2006) 418–428.
[49] M.C. van Teeseling, N.M. de Almeida, A. Klingl, D.R. Speth, H.J. Op den Camp, R. Rachel, M.S. Jetten, L. van Niftrik, A new addition to the cell plan of anammox bacteria: "*Candidatus* Kuenenia stuttgartiensis" has a protein surface layer as the outermost layer of the cell, J. Bacteriol. 196 (2014) 80–89.
[50] I. Wittig, T. Beckhaus, Z. Wumaier, M. Karas, H. Schägger, Mass estimation of native proteins by blue native electrophoresis: principles and practical hints, Mol. Cell. Proteomics 9 (2010) 2149–2161.
[51] M.H. Farhoud, H.J. Wessels, P.J. Steenbakkers, S. Mattijssen, R.A. Wevers, B.G. van Engelen, M.S. Jetten, J.A. Smeitink, L.P. van den Heuvel, J.T. Keltjens, Protein complexes in the archaeon *Methanothermobacter thermautotrophicus* analyzed by blue native/SDS-PAGE and mass spectrometry, Mol. Cell. Proteomics 4 (2005) 1653–1663.
[52] H.J. Wessels, T.G. Bloemberg, M. van Dael, R. Wehrens, L.M. Buydens, L.P. van den Heuvel, J. Gloerich, A comprehensive full factorial LC-MS/MS proteomics benchmark data set, Proteomics 12 (2012) 2276–2281.
[53] A. Shevchenko, M. Wilm, O. Vorm, M. Mann, Mass spectrometric sequencing of proteins from silver-stained polyacrylamide gels, Anal. Chem. 68 (1996) 850–858.
[54] J. Cox, M. Mann, MaxQuant enables high peptide identification rates, individualized p.p.b.-range mass accuracies and proteome-wide protein quantification, Nat. Biotechnol. 26 (2008) 1367–1372.
[55] A.I. Saeed, V. Sharov, J. White, J. Li, W. Liang, N. Bhagabati, J. Braisted, M. Klapa, T. Currier, M. Thiagarajan, A. Sturn, M. Snuffin, A. Rezantsev, D. Popov, A. Ryltsov, E. Kostukovich, I. Borisovsky, Z. Liu, A. Vinsavich, V. Trush, J. Quackenbush, TM4: a free, open-source system for microarray data management and analysis, Biotechniques 34 (2003) 374–378.
[56] T.N. Petersen, S. Brunak, G. von Heijne, H. Nielsen, SignalP 4.0: discriminating signal peptides from transmembrane regions, Nat. Methods 8 (2011) 785–786.
[57] A. Krogh, B. Larsson, G. von Heijne, E.L. Sonnhammer, Predicting transmembrane protein topology with a hidden Markov model: application to complete genomes, J. Mol. Biol. 305 (2001) 567–580.
[58] J.D. Thompson, D.G. Higgins, T.J. Gibson, CLUSTAL W: improving the sensitivity of progressive multiple sequence alignment through sequence weighting, position-specific gap penalties and weight matrix choice, Nucleic Acids Res. 22 (1994) 4673–4680.
[59] J. Söding, A. Biegert, A.N. Lupas, The HHpred interactive server for protein homology detection and structure prediction, Nucleic Acids Res. 33 (2005) W244–W248.
[60] L. van Niftrik, M. van Helden, S. Kirchen, E.G. van Donselaar, H.R. Harhangi, R.I. Webb, J.A. Fuerst, H.J. Op den Camp, M.S. Jetten, M. Strous, Intracellular localization of membrane-bound ATPases in the compartmentalized anammox bacterium '*Candidatus* Kuenenia stuttgartiensis', Mol. Microbiol. 77 (2010) 701–715.
[61] M.C. van Teeseling, R.J. Mesman, E. Kuru, A. Espaillat, F. Cava, Y.V. Brun, M.S. Van Nieuwenhuize, B. Kartal, L. van Niftrik, Anammox Planctomycetes have a peptidoglycan cell wall, Nat. Commun. 6 (2015) 6878.
[62] M. Ali, M. Oshiki, T. Awata, K. Isobe, Z. Kimura, H. Yoshikawa, D. Hira, T. Kindaichi, H. Satoh, T. Fujii, S. Okabe, Physiological characterization of anaerobic ammonium oxidizing bacterium "*Candidatus* Jettenia caeni", Environ. Microbiol. 17 (2015) 2172–2189.
[63] V.B. Borisov, R.B. Gennis, J. Hemp, M.I. Verkhovsky, The cytochrome *bd* respiratory oxygen reductases, Biochim. Biophys. Acta 1807 (2011) 1398–1413.
[64] S. Safarian, C. Rajendran, H. Müller, J. Preu, J.D. Langer, S. Ovchinnikov, T. Hirose, T. Kusumoto, J. Sakamoto, H. Michel, Structure of a *bd* oxidase indicates similar mechanisms for membrane-integrated oxygen reductases, Science 352 (2016) 583–586.
[65] A. Reyes-Prieto, B. Barquera, O. Juárez, Origin and evolution of the sodium-pumping NADH: ubiquinone oxidoreductase, PLoS One 9 (2014) e96696.
[66] R.G. Efremov, L.A. Sazanov, The coupling mechanism of respiratory complex I – a structural and evolutionary perspective, Biochim. Biophys. Acta 1817 (2012) 1785–1795.
[67] B.C. Marreiros, A.P. Batista, A.M. Duarte, M.M.A. Pereira, A missing link between complex I and group 4 membrane-bound [NiFe] hydrogenases, Biochim. Biophys. Acta 1827 (2013) 198–209.
[68] G.J. Schut, O. Zadvornyy, C.H. Wu, J.W. Peters, E.S. Boyd, M.W. Adams, The role of geochemistry and energetics in the evolution of modern respiratory complexes from a proton-reducing ancestor, Biochim. Biophys. Acta 1857 (2016) 958–970.
[69] J. Steuber, G. Vohl, M.S. Casutt, T. Vorburger, K. Diederichs, G. Fritz, Structure of the *V. cholerae* Na^+-pumping NADH:quinone oxidoreductase, Nature 516 (2014) 62–67.
[70] E. Biegel, S. Schmidt, J.M. González, V. Müller, Biochemistry, evolution and physiological function of the Rnf complex, a novel ion-motive electron transport complex in prokaryotes, Cell. Mol. Life Sci. 68 (2011) 613–634.
[71] D.V. Dibrova, M.Y. Galperin, A.Y. Mulkidjanian, Characterization of the N-ATPase, a distinct, laterally transferred Na^+-translocating form of the bacterial F-type membrane ATPase, Bioinformatics 26 (2010) 1473–1476.
[72] L.A. Eichacker, B. Granvogl, O. Mirus, B.C. Müller, C. Miess, E. Schleiff, Hiding behind hydrophobicity. Transmembrane segments in mass spectrometry, J. Biol. Chem. 279 (2004) 50915–50922.
[73] A.O. Helbig, A.J. Heck, M. Slijper, Exploring the membrane proteome–challenges and analytical strategies, J. Proteome 73 (2010) 868–878.
[74] I. Wittig, H. Schägger, Supramolecular organization of ATP synthase and respiratory chain in mitochondrial membranes, Biochim. Biophys. Acta 1787 (2009) 672–680.
[75] M.L. Genova, G. Lenaz, Functional role of mitochondrial respiratory supercomplexes, Biochim. Biophys. Acta 1837 (2014) 427–443.
[76] A.M. Melo, M. Teixeira, Supramolecular organization of bacterial aerobic respiratory chains: From cells and back, Biochim. Biophys. Acta 1857 (2016) 190–197.
[77] A. Magalon, R. Arias-Cartin, A. Walburger, Supramolecular organization in prokaryotic respiratory systems, Adv. Microb. Physiol. 61 (2013) 217–266.
[78] J. Simon, M.G. Klotz, Diversity and evolution of bioenergetic systems involved in microbial nitrogen compound transformations, Biochim. Biophys. Acta 1827 (2013) 114–135.
[79] W.A. Cramer, S.S. Hasan, E. Yamashita, The Q cycle of cytochrome *bc* complexes: a structure perspective, Biochim. Biophys. Acta 1807 (2011) 788–802.
[80] D.V. Dibrova, D.A. Cherepanov, M.Y. Galperin, V.P. Skulachev, A.Y. Mulkidjanian, Evolution of cytochrome *bc* complexes: from membrane-anchored dehydrogenases of ancient bacteria to triggers of apoptosis in vertebrates, Biochim. Biophys. Acta 1827 (2013) 1407–1427.
[81] A.N. Tikhonov, The cytochrome b_6f complex at the crossroad of photosynthetic electron transport pathways, Plant Physiol. Biochem. 81 (2014) 163–183.
[82] T. Shikanai, Central role of cyclic electron transport around photosystem I in the regulation of photosynthesis, Curr. Opin. Biotechnol. 26 (2014) 25–30.
[83] M.A. Schöttler, S.Z. Tóth, A. Boulouis, S. Kahlau, Photosynthetic complex stoichiometry dynamics in higher plants: biogenesis, function, and turnover of ATP synthase and the cytochrome b_6f complex, J. Exp. Bot. 66 (2015) 2373–2400.
[84] F. ten Brink, B. Schoepp-Cothenet, R. van Lis, W. Nitschke, F. Baymann, Multiple Rieske/cyt *b* complexes in a single organism, Biochim. Biophys. Acta 1827 (2013) 1392–1406.
[85] D.R. Speth, M.C. van Teeseling, M.S.M. Jetten, Genomic analysis indicates the presence of an asymmetric bilayer outer membrane in planctomycetes and verrucomicrobia, Front. Microbiol. 3 (2012) 304.